Is Arg418 the Catalytic Base Required for the Hydrolysis Step of the IMP Dehydrogenase Reaction?†

Yollete V. Guillén Schlippe‡ and Lizbeth Hedstrom*

Department of Biochemistry, Brandeis University, Waltham, Massachusetts 02454

Received August 3, 2004; Revised Manuscript Received July 8, 2005

ABSTRACT: The first committed step of guanine nucleotide biosynthesis is the oxidation of inosine 5′-monophosphate (IMP) to xanthosine 5′-monophosphate (XMP) catalyzed by IMP dehydrogenase. The reaction involves the reduction of NAD^+ with the formation of a covalent enzyme intermediate (E−XMP*). Hydrolysis of E−XMP* requires the enzyme to adopt a closed conformation and is rate-limiting. Thr321, Arg418, and Tyr419 are candidates for the residue that activates water. The substitution of Thr321 has similar, but small, effects on both the hydride transfer and hydrolysis steps. This result suggests that Thr321 influences the reactivity of Cys319, either through a direct interaction or by stabilizing the structure of the active site loop. The hydrolysis of E−XMP* is accelerated by the deprotonation of a residue with a pK_a of ∼8. A similar deprotonation stabilizes the closed conformation; this residue has a pK_a of ≥6 in the closed conformation. The substitution of Tyr419 with Phe does not change the pH dependence of either the hydrolysis of E−XMP* or the conformational change, which suggests that Tyr419 is not the residue that activates water. In contrast, the conformational change becomes pH-independent when Arg418 is substituted with Gln. Lys can replace the function of Arg418 in the hydrolysis reaction but does not stabilize the closed conformation. The simplest explanation for these observations is that Arg418 serves as the base that activates water in the IMPDH reaction.

Inosine 5′-monophosphate dehydrogenase (IMPDH)[1] catalyzes the oxidation of IMP to XMP using NAD^+ as the cofactor (Scheme 1). This reaction is the first committed and rate-limiting step in *de novo* guanine nucleotide biosynthesis (*1*). Inhibitors of IMPDH have antiproliferative activity and are used as immunosuppressive (*2*), anticancer (*3*), and antiviral agents (*4*). The reaction occurs in two steps (Scheme 1). (1) Cys319 attacks the C-2 position of IMP, and a hydride is transferred to form the covalent intermediate E−XMP* and NADH (*Tritrichomonas foetus* IMPDH numbering will be used throughout); NADH is released. (2) E−XMP* is hydrolyzed to produce XMP. The NADH release and hydrolysis steps are both partially rate-limiting (*5*). The enzyme undergoes an unusual conformational change in midcatalytic stream that controls drug selectivity. After NADH departs, a flap (residues 413−431) moves into the vacant dinucleotide site, switching the enzyme from the open conformation required for the hydride transfer reaction into the closed conformation needed for hydrolysis of E−XMP* (Scheme 2) (*6*). Drugs such as mizoribine monophosphate (MZP) induce the closed conformation (*6*, *7*), while others like mycophenolic acid (MPA) compete with the flap for the dinucleotide site (*8*).

Hydrolases usually contain a His, Asp, Glu, or Lys residue that acts as a general base to activate water. Substitution of these residues typically decreases the rate of hydrolysis by factors of $100-10^5$. Surprisingly, none of the usual residues are positioned to activate water in the IMPDH reaction. Instead, two flap residues, Arg418 and Tyr419, form hydrogen bonds with a putative catalytic water molecule in the E·MZP complex (Figure 1A; *6*). Arg418 also interacts with the dinucleotide binding site, forming a hydrogen bond to Asp261. In the open conformation, Asp261 makes hydrogen bonds to the hydroxyl groups of the nicotinamide ribose of NAD^+ (*9*). Asp261, Arg418, and Tyr419 may form a triad that cooperates to activate water. Thr321 also appears to form a hydrogen bond to the catalytic water in the E·MZP complex (Figure 1A; *6*), suggesting that this residue may activate water as originally proposed by Sintchak and colleagues (*10*). However, Thr321 is also in position to make a hydrogen bond to Cys319 in the E·MZP complex and has alternative conformations in other complexes such as E·IMP·TAD, where it forms a hydrogen bond to Gly314 that may stabilize the structure of the active site loop (Figure 1B; *9*). It is difficult to determine which of these interactions are relevant to catalysis. In any case, Thr321, Arg418, and Tyr419 are expected to have high pK_as (13, 12.5, and 10 for Thr, Arg, and Tyr residues, respectively) and thus are all unlikely candidates to serve as the base that activates water in the IMPDH reaction.

† Supported by NIH Grant GM54403 (L.H.) and NIH Training Grant GM08417 (Y.V.G.S.).

* To whom correspondence should be addressed. Telephone: (781) 736-2333. Fax: (781) 736-2349. E-mail: hedstrom@brandeis.edu.

‡ Current address: Department of Molecular Biology, Massachusetts General Hospital, Boston, MA 02114.

[1] Abbreviations: IMPDH, inosine 5′-monophosphate dehydrogenase; IMP, inosine 5′-monophosphate; MPA, mycophenolic acid; MZP, mizoribine 5′-monophosphate; NAD^+, nicotinamide adenine dinucleotide; NADH, reduced nicotinamide adenine dinucleotide; XMP, xanthosine 5′-monophosphate; LDH, lactate dehydrogenase; tiazofurin, 2-β-D-ribofuranosylthiazole-4-carboxamide; DTT, dithiothreitol; TAD, thiazole-4-carboxamide adenine dinucleotide; SIE, solvent isotope effect.

10.1021/bi048342v CCC: $30.25
Published on Web 08/09/2005

Scheme 1: Chemical Mechanism of IMPDH[a]

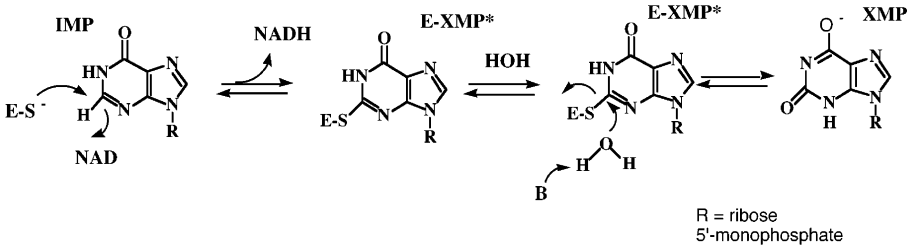

[a] The active site Cys attacks C-2 of IMP, and a hydride is transferred to NAD^+ to form E−XMP* and NADH. NADH is released before the hydrolysis of E−XMP*.

Scheme 2: Kinetic Mechanism of the IMPDH Reaction[a]

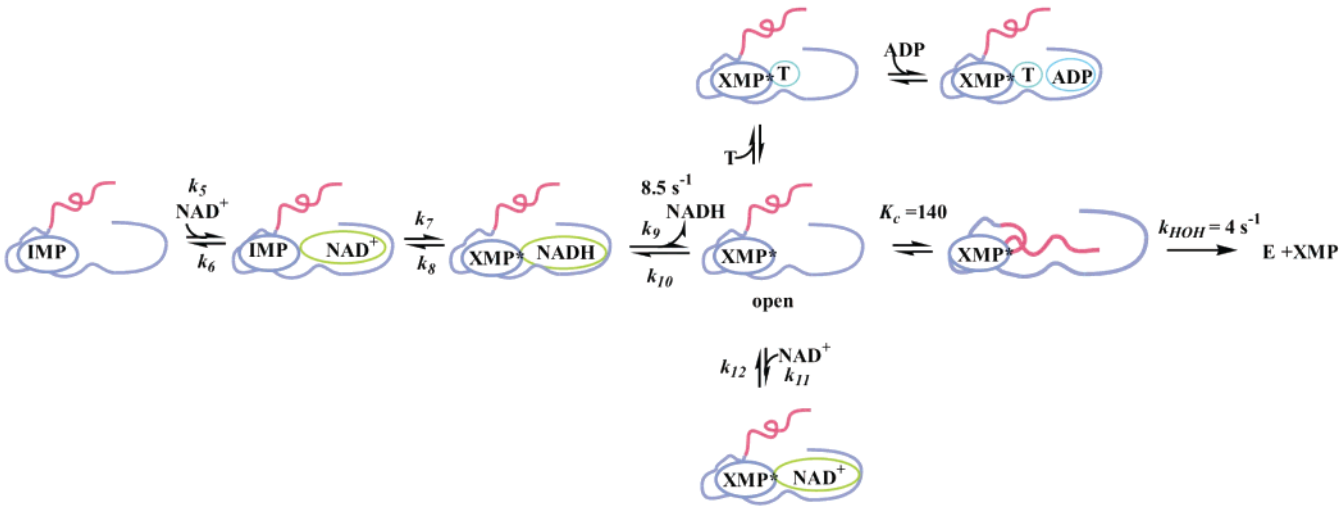

[a] The reaction involves random addition of substrates; the scheme starts with the E·IMP complex because this is the complex used to initiate the pre-steady-state experiments described in the text. The rate constants and/or equilibrium constant for the wild-type enzyme are shown for the NADH release, conformational change, and hydrolysis steps. The scheme also depicts substrate inhibition due to formation of the E−XMP*·NAD^+ complex and the interaction of tiazofurin (T) and ADP. If the closed conformation is favored, the first inhibitor will induce the open conformation, favoring the binding of the second inhibitor, and a synergistic interaction will be observed.

Mutagenesis experiments provide some further insights into the function of Asp261, Arg418, Tyr419, and Thr321. The substitution of Asp261 with Ala in *Escherichia coli* IMPDH decreases the value of k_{cat} by a factor of 130, the value of K_d for the NAD^+ analogue TAD by a factor of 25, and the K_d for MZP by a factor of 80 (*11*). These observations suggest that Asp261 influences both the hydride transfer and hydrolysis steps as suggested by the X-ray crystal structures. In contrast, the Arg418Ala and Tyr419Phe mutations of *T. foetus* IMPDH have no effect on hydride transfer but do selectively impair the hydrolysis of E−XMP* (*6*, *12*). The Arg418Ala substitution decreases the value of k_{HOH} by a factor of 500, a magnitude consistent with the role of the base that activates water (see Scheme 2 for definitions of rate constants). The Tyr419Phe mutation decreases the value of k_{HOH} by a factor of only 20, so this residue does not play a major role in water activation. Both the Arg418Ala and Tyr419Phe substitutions also destabilize the closed conformation, although not to the extent that the open conformation is favored [i.e., K_c remains ≥1 (*12*)]. The role of Thr321 was investigated in human IMPDH type 2, where the Thr321Ala substitution decreases the value of k_{cat} by a factor of only 20 (*13*). Although the effects of this mutation on individual rate constants have not been determined, this observation suggests that Thr321 has at most a minor role in the hydrolysis reaction.

Here we further investigate the roles of Thr321, Arg418, and Tyr419 in the IMPDH reaction. These experiments suggest that Thr321 does not activate water but instead influences the reactivity of Cys319, either through a direct interaction or by stabilizing the structure of the active site loop. The pH dependence of the reaction suggests that a residue with a pK_a of ∼8 in the closed form and ≥10 in the open form modulates both the conformational change and the hydrolysis of E−XMP*. This residue is not Tyr419, but might be Arg418. The simplest explanation for these observations is that Arg418 acts as a base to activate water.

MATERIALS AND METHODS

Materials. IMP, ADP, NADH, and Tris were purchased from Sigma (St. Louis, MO). NAD^+ was purchased from Boehringer Mannheim. DTT was purchased from Research Organics, Inc. D_2O, KOD, and DCl were purchased from Cambridge Isotope Laboratories, Inc. LDH (bovine heart) was purchased from ICN Biomedicals, Inc. Tiazofurin was obtained from NCI. Oligonucleotides were purchased from Operon and Integrated DNA Technologies, Inc.

Site-Directed Mutagenesis. The Arg418His, Arg418Lys, Arg418Gln, and Thr321Ala mutations were constructed in *T. foetus* IMPDH using the Quikchange kit (Stratagene, La Jolla, CA) (*5*). The entire coding sequences were sequenced to ensure that no undesired mutations were introduced.

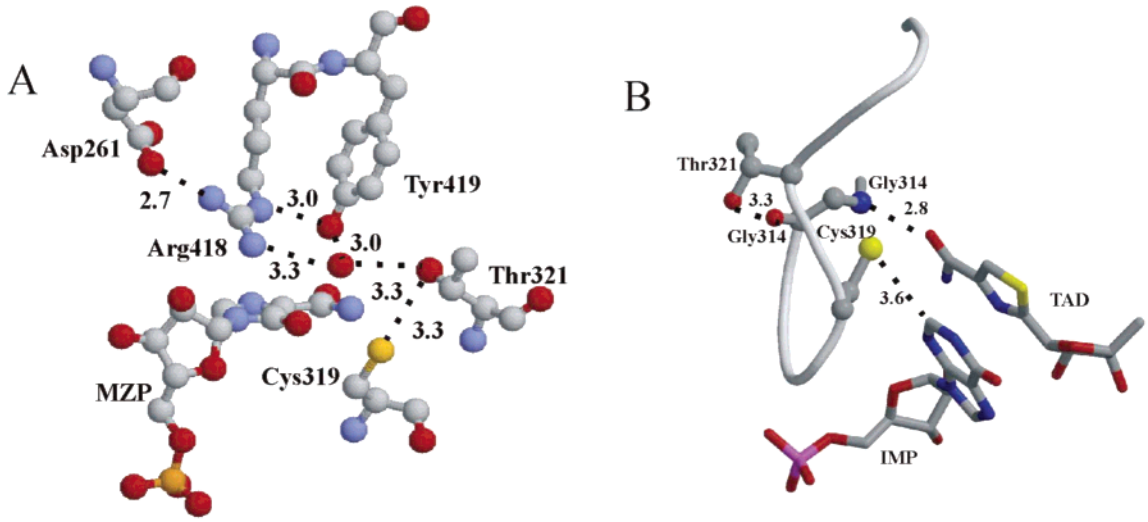

FIGURE 1: Interactions of the Arg418-Tyr419 dyad and Thr321 in *T. foetus* IMPDH. The numbers denote distances between atoms in angstroms. (A) Interactions in the E·MZP complex (*6*). The side chains of Thr321, Arg418, Tyr419, and Cys319 are shown as well as the inhibitor MZP and water 241. Atoms are colored as follows: gray for C, blue for N, red for O, gold for S, and orange for P. This panel was generated with RasWin Molecular Graphics and rendered with CorelDRAW 9. (B) Interactions of Thr321 in the E·TAD·IMP complex (*9*). The side chains of Thr321 and Cys319 and the backbone amide and carbonyl oxygen of Gly314 are shown as well as the inhibitor TAD and the substrate IMP. This panel was created with MolScript and rendered with Raster3D and CorelDRAW 9 (*27*, *28*). Atoms are colored as described above except P (purple).

Plasmids containing the mutant IMPDH gene were transformed and expressed in *E. coli* H712 cells, which lack endogenous IMPDH (*14*). Arg418Lys, Arg418Gln, and Thr321Ala were purified as previously described (*12*). Arg418His is unstable and could not be purified.

Enzyme Kinetics. Standard IMPDH assays contained saturating concentrations of IMP (from 100 μM to 2 mM) and varying concentrations of NAD^+ in 100 mM KCl, 3 mM EDTA, 1 mM DTT, and 50 mM Tris-HCl (pH 8.0) (assay buffer). All assays were performed at 25 °C. Assays of the Arg418 mutants contained LDH (20 μM) to scavenge NADH and alleviate product inhibition (*12*). Activity was measured by monitoring the fluorescence of NADH (λ_{ex} = 340 nm, λ_{em} = 460 nm) on a PerSeptive Biosystems Cytofluor II multiwell plate reader. Rates of NADH production were determined by calibration of the instrument with a standard curve of NADH solution in assay buffer containing LDH. The presence of NAD^+ does not affect the fluorescence of NADH under these conditions. The reaction of Thr321Ala was assayed by monitoring the absorbance of NADH at 340 nm (ϵ_{340} = 6.22 mM^{-1} cm^{-1}) on a Hitachi U-2000 UV−visible spectrophotometer. Steady-state parameters with respect to NAD^+ were derived at saturating IMP concentrations by plotting the initial velocity against NAD^+ concentration and fitting to an equation describing uncompetitive substrate inhibition (eq 1) using SigmaPlot (SPSS, Inc.):

$$v = V_m/(1 + K_a/[NAD^+] + [NAD^+]/K_{ii}) \quad (1)$$

where v is the initial velocity, V_m is the maximal velocity, K_a is the Michaelis constant, and K_{ii} is the substrate inhibition constant for NAD^+.

pH Dependence of Wild-Type and Tyr419Phe IMPDH. Assay mix was prepared as described above except the following buffers were substituted: potassium MOPS for pH 6.0−7.0, potassium TES for pH 7.0−7.75, Tris-HCl for pH 8.0, GlyGly-HCl for pH 8.0−9.0 (wild type), MES for pH 5.5−6.5, and Tris-HCl for pH 7.0−9.0 (Tyr419Phe). The concentration of IMP was fixed at 2 mM, and the concentration of NAD^+ was varied appropriately. The data were fitted to the following equations using SigmaPlot:

$$\log(V_m/K_m) = \log(V_m/K_m)_{indep} - \log(1 + [H^+]/K_a + K_b/[H^+]) \quad (2)$$

$$\log(V_m) = \log(V_m)_{indep} - \log(1 + [H^+]/K_a) \quad (3)$$

where $(V_m/K_m)_{app}$ and $(V_m)_{app}$ are the apparent values at each pH, $(V_m/K_m)_{indep}$ and $(V_m)_{indep}$ are the pH-independent values, K_a is the acid dissociation constant for the most acidic ionization, and K_b is the acid dissociation constant for the most basic ionization.

Pre-Steady-State Kinetics. Pre-steady-state experiments were performed using an Applied Photophysics SX.17MV stopped-flow spectrophotometer. NADH production was monitored by either absorbance (340 nm wavelength), which monitors both free and bound NADH, or fluorescence (λ_{ex} = 340 nm, 420 nm cutoff emission filter), which detects only free NADH (*5*). Enzyme was preincubated with saturating concentrations of IMP and mixed with an equal volume of varying concentrations of NAD^+ to give final concentrations of 100 μM IMP and 0.5−2.4 μM IMPDH. Progress curves were fitted to either a single-exponential (eq 4) or double-exponential (eq 5) equation with a steady-state term:

$$S_t = A_1[1 - \exp(-k_{obs1}t)] + vt + B \quad (4)$$

$$S_t = A_1[1 - \exp(-k_{obs1}t)] + A_2[1 - \exp(-k_{obs2}t)] + vt + B \quad (5)$$

where S_t is the signal at time t, A_1 and A_2 are the amplitudes of the first and second phases, respectively, k_{obs1} and k_{obs2} are the observed first-order rate constants for the first and second phases, respectively, v is the steady-state rate of the

Scheme 3: pH Dependence of the Conformational Change

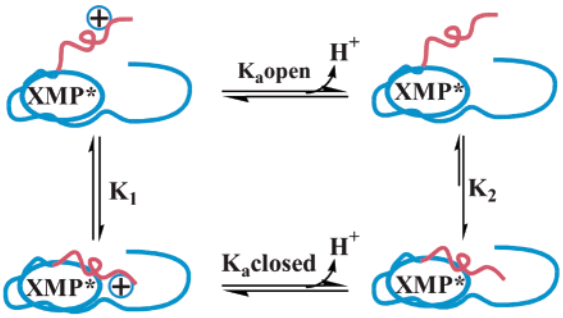

linear increase in absorbance or fluorescence, and B is the background signal at time zero. Where appropriate, the values of k_{obs} and amplitude were fitted to eqs 6 and 7:

$$k_{obs} = k_{burst}[NAD^+]/(K_{app} + [NAD^+]) \quad (6)$$

$$A_1 = Amp_1[NAD^+]/(K_{app} + [NAD^+]) \quad (7)$$

where k_{burst} is the maximal value of k_{obs} and Amp_1 is the maximal value of A_1. The progress curve for the reactions of Arg418Lys was not described well by either eq 4 or 5 due to severe NADH inhibition. Therefore, the progress curves were globally fit to the mechanism shown in Scheme 2 using Dynafit software as previously described (*12*, *15*). The rate constants for the binding of IMP and XMP were fixed at wild-type values (*5*), and the conformational change and hydrolysis steps (K_c and k_{HOH}) were combined into one composite step (k_{comp}).

Solvent Deuterium Isotope Effects. Assay buffer and substrates were prepared in D_2O or H_2O. The pH meter readings were corrected to pD by adding 0.4 (*16*). Activity was assayed at saturating IMP concentrations (from 100 μM to 2 mM), while NAD^+ concentrations were varied appropriately. For the wild-type reaction, pD was varied using the same buffers as described above.

Multiple-Inhibitor Kinetics. Multiple-inhibitor experiments with tiazofurin and ADP were performed at constant IMP (100 μM) and NAD^+ concentrations (20 and 530 μM for Arg418Ala and Arg418Gln, respectively). Initial velocities were fit to eq 8:

$$v = v_0/(1 + [I]/K_i + [J]/K_j + [I][J]/\alpha K_i K_j) \quad (8)$$

where v is the initial velocity, v_0 is the initial velocity in the absence of inhibitor, K_i and K_j are the inhibition constants for the inhibitors I and J, respectively, and α is the interaction constant. In wild-type IMPDH, the tiazofurin and ADP are strongly synergistic inhibitors with an interaction constant α of 0.007 (*17*, *18*). This observation suggests that one inhibitor shifts the enzyme into the open conformation, thus promoting the association of the second inhibitor (Scheme 2; *12*). Further, the value of α approximates the fraction of enzyme in the open conformation, so the value of K_c can be obtained (*12*):

$$K_c = (1 - \alpha)/\alpha \quad (9)$$

Given the mechanism of Scheme 3, the pH dependence of

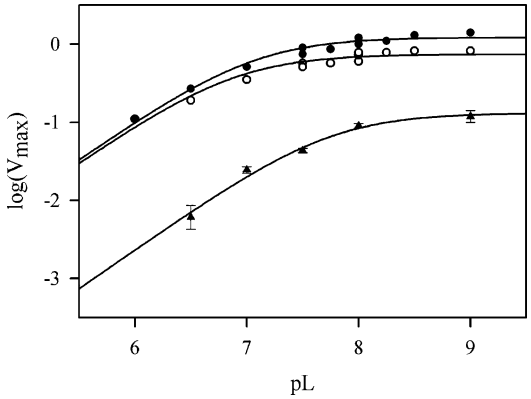

FIGURE 2: pH dependence of V_{max}. The values of V_{max} were determined by measuring initial rates at saturating IMP concentrations and varying concentrations of NAD^+. The data were fit as described in Materials and Methods. The filled circles denote the wild-type reaction in H_2O, V_{max}, where $pK_a = 7.0 \pm 0.2$. The empty circles denote the wild-type reaction in D_2O, V_{max}, where $pK_a = 7.1 \pm 0.1$. The triangles denote the reaction of Tyr419Phe in H_2O, where $pK_a = 7.7 \pm 0.1$.

K_c is described by eq 10 (derivation in the Supporting Information):

$$\log(K_c) = \log[K_1K_2(K_{a\ closed} + [H^+])] - \log(K_1K_{a\ closed} + K_2[H^+]) \quad (10)$$

where K_1 describes the equilibrium between open and closed conformations for the protonated enzyme, K_2 describes the equilibrium between open and closed conformations for the protonated enzyme, and $K_{a\ closed}$ is the acid dissociation constant for the closed conformation.

RESULTS AND DISCUSSION

pH Dependence of the IMPDH Reaction. We investigated the dependence of the IMPDH reaction on pH and pD to gain more insight into the mechanism of IMPDH. The reaction of *T. foetus* IMPDH displays a dependence on pH similar to that previously reported for the human enzyme (*19*). This paper addresses the mechanism of the hydrolysis reaction, so discussion will focus on the pH−rate profile of V_{max}. The pH−rate profile of V/K_m(NAD) is included in the Supporting Information (Figure S1). The pH dependence of V_m displays a single pK_a of 7.0 ± 0.1 (Figure 2), which could derive from the ionization of a residue involved in hydride transfer, NADH release, the conformational change, or hydrolysis of E−XMP*.

The pre-steady-state reaction was investigated by monitoring the production of NADH by absorbance (which detects free and enzyme-bound NADH) and fluorescence (which detects only free NADH) to determine which of these steps are pH-dependent. A burst of absorbance at 340 nm is observed at all pH values, indicating that hydride transfer is not rate-limiting ($k_{obs} > 30\ s^{-1}$, for the reaction of 100 μM IMP and 10 mM NAD^+ at pH 5.5−9). A burst of NADH production is also observed when fluorescence is monitored at all pH values, indicating that NADH release is pH-independent ($k_9 \sim 8\ s^{-1}$). These observations indicate that the steps involved in the hydrolysis of E−XMP*, K_c and k_{HOH}, are rate-limiting at low pH; as the pH increases, NADH release also limits the reaction. Therefore, the pK_a of 7.0 is

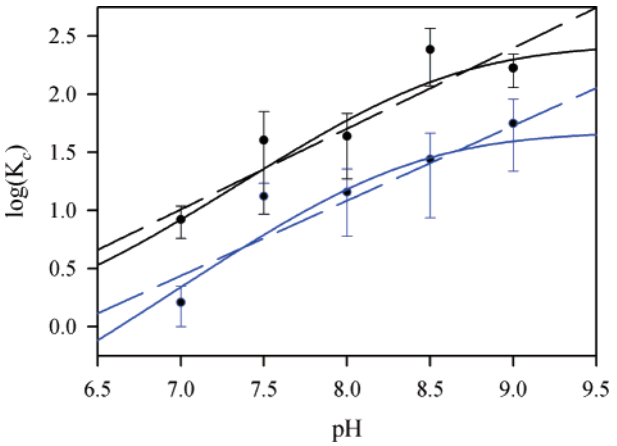

FIGURE 3: Dependence of K_c on pH: wild type (black) and Tyr419Phe (blue). The values of K_c were determined using multiple-inhibitor experiments as described in Materials and Methods. $[NAD^+] = 500$ and 250 μM for wild-type and Arg418Gln enzymes, respectively, and LDH was omitted. Linear regression gives a slope of 0.7 ± 0.1 ($R = 0.86$) for the wild type and a slope of 0.7 ± 0.1 ($R = 0.84$) for the Tyr419Phe variant. Also shown are the best fits to eq 10 describing Scheme 3. For the wild-type enzyme, $pK_{a\ closed} = 6 \pm 2$, $K_1 = 1 \pm 6$, and $K_2 = 270 \pm 170$ ($R = 0.88$). For the Tyr419Phe variant, $pK_{a\ closed} = 6 \pm 8$, $K_1 = 0.1 \pm 2$, and $K_2 = 48 \pm 24$ ($R = 0.85$). These values are underdetermined since the data do not extend into the pH-independent regions, but nevertheless represent useful limits.

a lower limit for the pK_a of some Residue X involving K_c and/or k_{HOH}. However, if NADH release becomes completely rate limiting, the value of k_{cat} should increase by a factor of ~2 between pH 8 and 9 (Table 2). The observed increase is only 40%, which suggests that the pK_a of Residue X must be ~8.

Solvent Isotope Effects on V_{max}. A similar pK_a is observed when the reaction is performed in D_2O ($pK_a = 7.1 \pm 0.1$; Figure 2). The values of pK_a of oxygen and nitrogen bases usually shift ~0.5 in D_2O (*16*), which further suggests that the pK_a of ~7 is the lower limit for ionization of Residue X. A normal SIE of 1.5 ± 0.2 is observed on V_m, which is in good agreement with that previously reported at pH 8.0 (*12*, *18*). An intrinsic SIE on the k_{HOH} of ~2 can be estimated using the rate constants listed in Table 2. A normal SIE of this magnitude is consistent with the operation of general base catalysis during the hydrolysis of E−XMP* (*16*). Therefore, the simplest explanation for the SIE on V_{max} is rate-limiting transfer of a proton from water to a general base during the hydrolysis of E−XMP*.

pH Dependence of K_c. Multiple-inhibitor experiments were used to measure K_c as outlined in Materials and Methods. The value of K_c increases with an increase in pH (Figure 3), which suggests that the deprotonation of Residue X favors the closed conformation (Scheme 3; $K_2 > K_1$). The data are described well by a line with a slope of 0.7 ± 0.1, which places the following limits on the equilibrium and dissociation constants of Scheme 3: $K_1 \leq 5$, $K_2 \geq 250$, $pK_{a\ open} \geq 8$, and $pK_{a\ closed} \geq 6$. It is likely that $pK_{a\ closed}$ and the pK_a of ~8 in the pH−rate profile both derive from the ionization of the same Residue X. It is also likely that this pK_a derives from the base that activates water, which suggests that Residue X may be Thr321, Arg418, or Tyr419.

Thr321 Is Involved in both the Hydride Transfer and Hydrolysis Reactions. We constructed the Thr321Ala mutation in *T. foetus* IMPDH to investigate the role of Thr321 in the IMPDH reaction. This mutation causes a 10-fold decrease in the value of k_{cat} (Table 1; for comparison, we have included the parameters for Arg418Ala and Tyr419Phe from ref *12*). The pre-steady-state reaction was monitored to determine which steps are altered by this mutation. Similar bursts of NADH production are observed when the reaction is measured by absorbance, which detects both free and enzyme-bound NADH, and fluorescence, which detects only free NADH (*5*). Both progress curves are described well by a single-exponential function with a steady-state term ($k_{obs} \sim 1.5\ s^{-1}$ for the reaction of 100 μM IMP and 5 mM NAD^+; see Figure S1 of the Supporting Information). The simplest explanation for these results is that NADH release is much faster than hydride transfer, which allows the following values to be assigned to the mechanistic rate constants of Scheme 2: $k_7 \sim 1.5\ s^{-1}$ and $k_9 \geq 8\ s^{-1}$. Therefore, k_{cat} is determined by the values of K_c and k_{HOH}.

High concentrations of NAD^+ inhibit IMPDH by competing with the flap for the NADH site of E−XMP* (Scheme 2). Substitutions that shift the equilibrium to the open conformation favor NAD^+ substrate inhibition. The Thr321Ala mutation decreases the value of $K_{ii}(NAD^+)$ by a factor of 7, which suggests that the fraction of enzyme in the open conformation has increased 7-fold and K_c is ~20. This value is best considered a lower limit for K_c, since the mutation is near the NAD^+ site and may also change the affinity of NAD^+ binding. Therefore, since the enzyme is predominantly in the closed conformation, $k_{cat} = k_{HOH} = 0.18\ s^{-1}$. These results indicate that the mutation of Thr321 impairs both hydride transfer and hydrolysis by a factor of ~20. These observations are therefore inconsistent with the postulate that Thr321 acts as the base to activate water. Instead, these dual effects suggest that Thr321 may activate Cys319 for nucleophillic attack and leaving group departure, either via a direct interaction or by stabilizing the structure of the active site loop (Figure 1). These observations combined with the high pK_a of Thr residues suggest that Residue X is not Thr321.

pH Dependence of the Tyr419Phe Variant. To determine if Residue X is Tyr419, we investigated the pH dependence of V_{max} for the reaction of the Tyr419Phe variant. A single pK_a of 7.7 ± 0.1 is observed (Figure 2). Since this mutation does not affect hydride transfer or NADH release (*12*), the hydrolysis of E−XMP* must be rate-limiting for this reaction. The simplest explanation of the data is that the substitution of Tyr419 does not influence the ionization of Residue X. Unlike that of the wild-type reaction, the value of k_9 is much greater than the value of k_{cat} at all pHs, so the pK_a of 7.7 can be assigned to the pK_a of Residue X.

As described above, multiple-inhibitor experiments were used to determine the pH dependence of K_c for the Tyr419Phe variant (Figure 3). The data parallel those for the wild-type reaction, which suggests that, although the magnitude of K_c is reduced by the Tyr419Phe substitution, it is modulated by the same ionization as the wild-type enzyme. These observations indicate that Tyr419 is not Residue X and further suggest that Tyr419 does not act as a base to activate water. In addition, these data suggest that the pK_a of Residue X is ~8 in the closed conformation and ≥10 in the open conformation.

Characterization of the Arg418Gln Mutation. Unfortunately, the low activity and severe product and substrate

Table 1: Kinetic Characterization of Wild-Type and Mutant IMPDHs

enzyme	k_{cat} (s^{-1})	K_m(IMP) (μM)	K_m(NAD^+) (μM)	K_{ii}(NAD^+) (mM)
wild-type[a]	1.9 ± 0.2	1.7 ± 0.4	150 ± 30	6.8 ± 1.8
Arg418Ala[b]	0.004 ± 0.0004	2.5 ± 2.8	1.6 ± 0.3	0.11 ± 0.014
Tyr419Phe[c]	0.22 ± 0.01	0.7 ± 0.9	70 ± 10	1.1 ± 0.2
Thr321Ala	0.18 ± 0.03	nd[d]	250 ± 60	0.90 ± 0.24
Arg418Gln	0.0069 ± 0.0014	nd[d]	300 ± 100	2.8 ± 1.1
Arg418Lys	0.15 ± 0.03	nd[d]	22 ± 6	0.021 ± 0.005

[a] These values are from ref *5*. [b] These values are from ref *12*. [c] Detection limit at 0.1 mM NAD^+ and 200 μM IMP. [d] Not determined.

Table 2: Mechanistic Rate Constants[a]

parameter	wild type[b,c]	Thr321Ala[d]	Arg418Ala[b,c]	Arg418Gln[d]	Arg418Lys[c]
k_5 (s^{-1} μM^{-1})	0.029	nd[f]	0.15	nd[f]	0.065[e]
k_6 (s^{-1})	4	nd[f]	3.8	nd[f]	3.4 ± 0.1
k_7 (s^{-1})	34	1.7	24	≥ 200	47 ± 1
k_8 (s^{-1})	59	na[g]	18	≥ 280	36 ± 1
k_9 (s^{-1})	8.5	≥ 8	11	≥ 4	6.5[e]
k_{10} (s^{-1} μM^{-1})	na[g]	na[g]	1.5	na[g]	4.8[e]
k_{11} (s^{-1} μM^{-1})	2	na[g]	0.0023	nd[f]	0.0053 ± 0.0001
k_{12} (s^{-1})	47	na[g]	0.0002	nd[f]	1.3[e]
K_c	140	≥ 20	1	10−50	≤ 0.1
k_{HOH} (s^{-1})	4	0.18	0.008	0.007	na[g]
k_{comp} (s^{-1})	na[g]	0.18	na[g]	na[g]	0.15

[a] Rate constants are defined in Scheme 2. k_{comp} denotes a composite rate constant combining K_c and k_{HOH}. [b] Values from ref *12*. [c] Values were derived from global analysis of progress curves comprising both pre-steady-state and steady-state reaction using DynaFit (*15*) as described in the Supporting Information of ref *12*. [d] Values deduced from pre-steady-state, steady-state, and inhibitor experiments as described in the text. [e] Errors are smaller than 2%. [f] Not determined. [g] Not applicable.

inhibition of the Arg418Ala variant preclude an investigation of the pH dependence this reaction. Therefore, we constructed the Arg418Gln variant to further investigate how Arg418 influences K_c and k_{HOH}. The activity of this mutant is comparable to that of Arg418Ala [$k_{cat} = 0.0069$ s^{-1} (Table 1)], and a similar SIE is observed [SIE $= 2.9 \pm 0.5$ vs 4.8 ± 2.0 (*12*)]. No SIE is observed on the values of K_i for tiazofurin and ADP, which suggests that the SIE does not result from an effect on K_c. This conclusion is further supported by multiple-inhibitor experiments with tiazofurin and ADP, where no SIE is observed on the value of the interaction constant α [SIE(α) $= 0.7 \pm 0.3$], so the SIE must result from an effect on k_{HOH}. Pre-steady-state experiments confirm that this mutation does not affect hydride transfer or NADH release (Table S1 of the Supporting Information and Table 3). Therefore, the Arg418Gln mutation specifically disrupts the hydrolysis step by decreasing K_c and/or k_{HOH}. The value of K_{ii}(NAD^+) is smaller than that of the wild type by a factor of 2.4 (Table 1), which suggests that $K_c \sim 50$ so that the enzyme is predominantly in the closed conformation. This conclusion was confirmed with a multiple-inhibitor experiment with an α of 0.03 and a K_c of $\sim$10. Modeling suggests that the side chain amide of Gln418 can simultaneously form hydrogen bonds to Asp261 and Tyr419 (Figure 4A), which can explain why the closed conformation is favored in this variant. These experiments demonstrate that the closed conformation is not sufficient for hydrolysis of E−XMP*. Importantly, if a residue other than Arg418 serves as the base that activates water, then the Arg418Gln variant should be more active than the Arg418Ala variant. This outcome is clearly not observed. In addition, these results demonstrate that the closed conformation does not require the presence of a positive charge at residue 418.

In contrast to those for the wild-type enzyme and Tyr419Phe variant, the value of K_c is pH-independent for the Arg418Gln enzyme (for pH 7.5, $\alpha = 0.025 \pm 0.017$; for pH 8.0, $\alpha = 0.033 \pm 0.027$; for pH 8.5, $\alpha = 0.025 \pm 0.015$; unfortunately, we can only measure a small pH range for technical reasons). This observation indicates that Arg418 governs the ionization of Residue X. The simplest explanation for this result is that Arg418 is Residue X.

The Nicotinamide Subsite Has a Preference for Neutral Ligands. If Residue X is Arg418, then the nictotinamide subsite of the dinucleotide site has a preference for uncharged ligands. This hypothesis is corroborated by the relative affinities of various NAD^+/NADH analogues. NADH binds more tightly than NAD^+ by a factor of 30 (*12*). TAD and benzamide dinucleotide also have much higher affinities than NAD^+ (*18*, *20*). Since the Arg418-Tyr419 dyad also binds in the nicotinamide subsite, it is reasonable to expect that the uncharged dyad will also be preferred.

Lys Can Substitute for Arg418. We constructed the Arg418Lys variant to further probe the role of Arg418 in the IMPDH reaction. Like the Arg418Ala and Arg418Gln variants, this enzyme is unable to complement IMPDH-deficient bacteria. Surprisingly, the purified Arg418Lys variant displayed significant IMPDH activity *in vitro*. Further characterization revealed that the enzyme is strongly inhibited by both NAD^+ and NADH (Table 1 and Figure S3 of the Supporting Information). The values of K_m(NAD^+) and K_{ii}-(NAD^+) are similar, so k_{cat} value of 0.15 s^{-1} is not well determined. The extremely low value of K_{ii}(NAD^+) suggests that the Arg418Lys variant is predominantly in the open conformation ($K_c \leq 0.1$). As expected, the Arg418Lys variant showed a pre-steady-state burst of NADH production when monitored by both absorbance and fluorescence. The progress curves showed two exponential phases followed by a nonlinear phase that is attributed to NADH product inhibition. The progress curves were globally fit to the kinetic mechanism shown in Scheme 2 using Dynafit (Table 3).

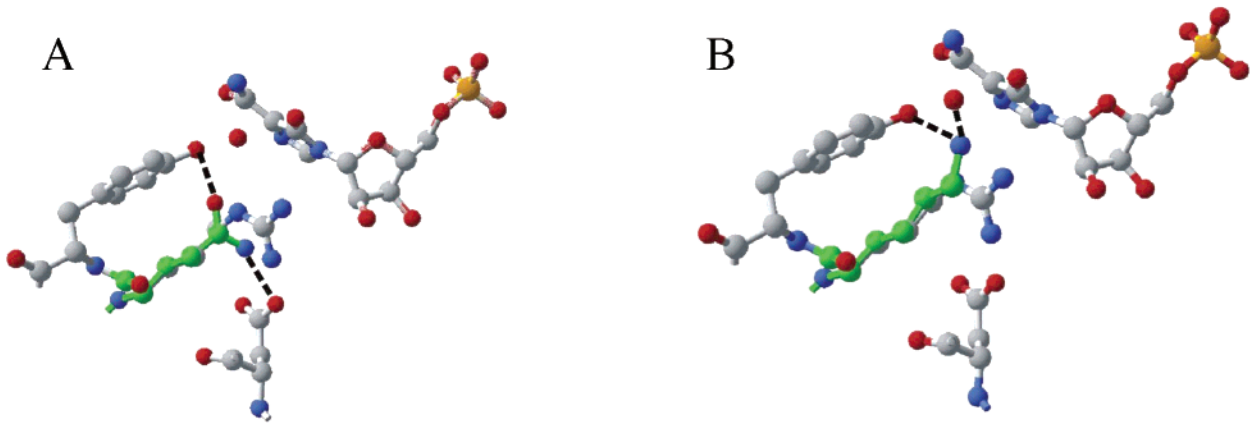

FIGURE 4: Model structures of the Arg418 mutants. (A) Model of Arg418Gln in the active site of the E·MZP complex (*6*). Atoms are colored as in Figure 1, except the carbon atoms of Gln418 are green. (B) Modeling of Arg418Lys into the active site of the E·MZP complex (*6*). Atoms are colored as described above, except the carbon atoms of Lys418 are green. Graphics were created in DeepView/Swiss-PdbViewer version 3.7 and rendered in CorelDraw version 9.

Hydride transfer and NADH release are similar to those of the wild type, as expected. The values of K_c and k_{HOH} could not be resolved and are therefore combined into a single rate constant ($k_{comp} = 0.15\ s^{-1}$), which agrees well with the k_{cat} of $0.15\ s^{-1}$ (Tables 1 and 3). The global analysis indicates that the rate constants for NAD^+ and NADH association (k_{10} and k_{11}, respectively) increase by factors of 2−3 relative to those of the Arg418Ala variant. This increase most likely results from an increase in the fraction of enzyme in the open conformation, again suggesting that $K_c \leq 0.1$. These observations suggest that $k_{HOH} \geq 1\ s^{-1}$, which is similar to that for the wild-type reaction (Table 2). Therefore, the Lys substitution is functionally equivalent to Arg418 once the closed conformation is formed. This result is surprising since Lys418 is not expected to be optimally oriented within the active site. Modeling suggests that the Lys substitution can form hydrogen bonds to both the catalytic water and Tyr419 (Figure 4B), and thus could replace Arg418. In addition, since the pK_a of Lys is ∼2−3 units lower than that of Arg, the fraction of Lys418 in the deprotonated form could exceed that of Arg418 by a factor of ∼100−1000, which may compensate for the imperfect orientation. It is interesting to note that although the Arg418Lys variant is an effective IMPDH *in vitro*, severe substrate and product inhibition make this enzyme an ineffective catalyst *in vivo*.

We also constructed Arg418His, but this protein precipitated under assay conditions; therefore, the activity of this mutant could not be assessed.

Does Arg418 Serve as the Base that Activates Water in the IMPDH Reaction? The experiments described above indicate that the closed conformation is stabilized by the deprotonation of a residue with a pK_a of ∼8. This deprotonation also controls k_{HOH}. This residue has a pK_a of ≥10 in the open conformation, and thus could be Thr321, Arg418, or Tyr419. However, substitution of either Thr321 or Tyr419 has only modest effects on k_{HOH}. Further, substitution of Tyr419 does not have a significant effect on the pH dependence of either K_c or k_{HOH}. In contrast, substitution of Arg418 has a large effect on k_{HOH} and changes the pH dependence of K_c. The simplest explanation for these observations is that the deprotonation of Arg418 stabilizes the closed conformation and controls k_{HOH}; i.e., the pK_a of Arg418 is ∼8 in the closed conformation.

How is the pK_a of Arg418 perturbed? There are no other positively charged residues near Arg418, and unlike carboxylate residues, hydrophobic environments do not lower the pK_as of amine and guanidinium groups; therefore, the usual mechanisms for perturbing pK_as do not appear to apply. In fact, Arg418 is adjacent to Asp261, which might be expected to increase its pK_a (although we note that the His residue in the catalytic triad of serine proteases has a normal pK_a despite its proximity to an Asp residue). Biochemistry textbooks usually attribute the high basicity of Arg residues to resonance stabilization and symmetry. Perhaps steric constraints and asymmetry within the active site combine to disrupt the resonance of the guanidinium group of Arg418. Interestingly, several natural products contain twisted guanidinium groups with pK_a values ranging from 7 to 8, demonstrating the effectiveness of this strategy (*21*, *22*). Precedence for this phenomenon can be found in dimethylarginine dimethylaminotransferase, which appears to twist the guanidine group of its substrate (*23*). Several other observations suggest that resonance stabilization may not be an adequate explanation for the high basicity of Arg residues (*24*). The barrier for rotation about the nitrogen bonds is rather low, which suggests that there is less double-bond character than would be expected. Protonation of guanidine is only ∼10 kcal/mol more exothermic than that of propylimine, which is much lower than expected if resonance stabilization was the major driving force. Last, the basicity of guanidine is similar to that of triethylamine in the gas phase, which indicates that the high basicity of guanidine in aqueous solution results from interactions with water. These observations suggest that simply removing an Arg residue from bulk water will lower its pK_a.

Arg residues also appear to act as bases in several enzymes that catalyze elimination reactions: fumarate reductase, L-aspartate oxidase, and polysaccharide lyases (*25*). Coincidently, although the structures are not related, all of these enzymes share a similar active site arrangement in which the catalytic Arg residue is within hydrogen bonding distance of a conserved Asp/Glu residue or a carboxylate group from the substrate and a Tyr residue is nearby. In all cases, a network of water molecules links these carboxylate residues to solvent (*25*), which suggests that the catalytic Arg residue may be part of a relay that transfers the proton to solvent.

These carboxylates might restrict hydrogen bonds to the catalytic Arg, forcing the guanidinium nitrogens into a tetrahedral geometry, disrupting resonance and lowering its pK_a. Bacteriorhodopsin provides one of the most dramatic, albeit controversial, examples of an Arg residue with an abnormally low pK_a. A recent time-resolved FT-IR investigation suggests that the pK_a of Arg82 is 5.8 in the M state (*26*). Arg82 is part of a network of hydrogen bonds that includes Tyr83, Glu194, and Glu204. Thus, the environment of the perturbed Arg82 of bacteriorhodopsin also has some commonalities with the active site of IMPDH. Obviously, there is much we do not understand about the ionization of guanidinium groups in proteins.

ACKNOWLEDGMENT

We thank Thomas Riera for helpful discussions and Akira Matsudafor providing EICARMP. We also acknowledge Stuart Endo-Streeter for assistance with Figure 1 and Becky Meyers of the Brandeis Core Facility for DNA sequencing.

SUPPORTING INFORMATION AVAILABLE

pH and pD dependence of V_{max}/K_m, velocity versus NAD^+ plot for Arg418Lys, pre-steady-state progress curves for Thr321Ala, pre-steady-state parameters, and derivation of the pH dependence of K_c. This material is available free of charge via the Internet at http://pubs.acs.org.

REFERENCES

1. Weber, G., Nakamura, H., Natsumeda, Y., Szekeres, T., and Nagai, M. (1992) Regulation of GTP biosynthesis, *Adv. Enzyme Regul. 32*, 57−69.
2. Allison, A. C., Kowalski, W. J., Muller, C. D., and Eugui, E. M. (1993) Mechanisms of action of mycophenolic acid, *Ann. N.Y. Acad. Sci. 696*, 63−87.
3. Weber, G. (1983) Biochemical strategy of cancer cells and the design of chemotherapy: G. H. A. Clowes memorial lecture, *Cancer Res. 43*, 3466−3492.
4. Robins, R. K., Revankar, G. R., McKernan, P. A., Murray, B. K., Kirsi, J. J., and North, J. A. (1985) The importance of IMP dehydrogenase inhibition in the broad spectrum antiviral activity of ribavirin and selenazofurin, *Adv. Enzyme Regul. 24*, 29−43.
5. Digits, J. A., and Hedstrom, L. (1999) Kinetic mechanism of *Tritrichomonas foetus* inosine-5′-monophosphate dehydrogenase, *Biochemistry 38*, 2295−2306.
6. Gan, L., Seyedsayamdost, M. R., Shuto, S., Matsuda, A., Petsko, G. A., and Hedstrom, L. (2003) The immunosuppressive agent mizoribine monophosphate forms a transition state analog complex with IMP dehydrogenase, *Biochemistry 42*, 857−863.
7. Kohler, G. A., Gong, X., Bentink, S., Theiss, S., Pagani, G. M., Agabian, N., and Hedstrom, L. (2005) The functional basis of mycophenolic acid resistance in *Candida albicans* IMP dehydrogenase, *J. Biol. Chem. 280*, 11295−11302.
8. Sintchak, M. D., Fleming, M. A., Futer, O., Raybuck, S. A., Chambers, S. P., Caron, P. R., Murcko, M., and Wilson, K. P. (1996) Structure and mechanism of inosine monophosphate dehydrogenase in complex with the immunosuppressant mycophenolic acid, *Cell 85*, 921−930.
9. Gan, L., Petsko, G. A., and Hedstrom, L. (2002) Crystal structure of a ternary complex of *Tritrichomonas foetus* inosine 5′-monophosphate dehydrogenase: NAD orients the active site loop for catalysis, *Biochemistry 41*, 13309−13317.
10. Sintchak, M. D., Badia, M. C., Futer, O., and Nimmesgern, E. (1999) X-ray crystal structure of the antiviral drug ribavirin monophosphate bound to IMP dehydrogenase, *Antiviral Res. 41*, A56.
11. Kerr, K. M., and Hedstrom, L. (1997) The roles of conserved carboxylate residues in IMP dehydrogenase and identification of a transition state analog, *Biochemistry 36*, 13365−13373.
12. Guillén Schlippe, Y. V., Riera, T. V., Seyedsayamdost, M. R., and Hedstrom, L. (2004) Substitution of the Conserved Arg-Tyr Dyad Selectively Disrupts the Hydrolysis Phase of the IMP Dehydrogenase Reaction, *Biochemistry 43*, 4511−4521.
13. Futer, O., Sintchak, M. D., Caron, P. R., Nimmesgern, E., DeCenzo, M. T., Livingston, D. J., and Raybuck, S. A. (2002) A mutational analysis of the active site of human type II inosine 5′-monophosphate dehydrogenase, *Biochim. Biophys. Acta 594*, 27−39.
14. Nijkamp, H. J. J., and De Haan, P. G. (1967) Genetic and biochemical studies of the guanosine 5′ monophosphate pathway in *Escherichia coli*, *Biochim. Biophys. Acta 145*, 31−40.
15. Kuzmic, P. (1996) Program DYNAFIT for the analysis of enzyme kinetic data: Application to HIV proteinase, *Anal. Biochem. 237*, 260−273.
16. Schowen, K. B., and Schowen, R. L. (1982) Solvent isotope effects on enzyme systems, *Methods Enzymol. 87*, 551−606.
17. Hedstrom, L., and Wang, C. C. (1990) Mycophenolic acid and thiazole adenine dinucleotide inhibition of *Tritrichomonas foetus* inosine 5′-monophosphate dehydrogenase: Implications on enzyme mechanism, *Biochemistry 29*, 849−854.
18. Digits, J. A., and Hedstrom, L. (2000) Drug selectivity is determined by coupling across the NAD^+ site of IMP dehydrogenase, *Biochemistry 39*, 1771−1777.
19. Markham, G. D., Bock, C. L., and Schalk-Hihi, C. (1999) Acid−base catalysis in the chemical mechanism of inosine monophosphate dehydrogenase, *Biochemistry 38*, 4433−4440.
20. Gharehbaghi, K., Grunberger, W., and Jayaram, H. N. (2002) Studies on the Mechanism of Action of Benzamide Riboside: A Novel Inhibitor of IMP Dehydrogenase, *Curr. Med. Chem. 9*, 743−748.
21. Sharma, G., and Magdoff-Fairchild, B. (1977) Natural products of marine sponges. 7. The constitution of weakly basic guanidine compounds, dibromophakellin and monobromophakellin, *J. Org. Chem. 42*, 4118−4124.
22. Rogers, R. S., and Rapoport, H. (1980) The pK_a's of saxitoxin, *J. Am. Chem. Soc. 102*, 7335−7339.
23. Murray-Rust, J., Leiper, J., McAlister, M., Phelan, J., Tilley, S., Santa Maria, J., Vallance, P., and McDonald, N. (2001) Structural insights into the hydrolysis of cellular nitric oxide synthase inhibitors by dimethylarginine dimethylaminohydrolase, *Nat. Struct. Biol. 8*, 679−683.
24. Raczynska, E. D., Cyranski, M. K., Gutowski, M., Rak, J., Gal, J.-F., Maria, P.-C., Darowska, M., and Duczmal, K. (2003) Consequences of proton transfer to guanidine, *J. Phys. Org. Chem. 16*, 91−106.
25. Guillen Schlippe, Y. V., and Hedstrom, L. (2005) A twisted base? The role of arginine in enzyme-catalyzed proton abstractions, *Arch. Biochem. Biophys. 433*, 266−278.
26. Xiao, Y., Hutson, M. S., Belenky, M., Herzfeld, J., and Braiman, M. S. (2004) Role of arginine-82 in fast proton release during the bacteriorhodopsin photocycle: A time-resolved FT-IR study of purple membranes containing ^{15}N-labeled arginine, *Biochemistry 43*, 12809−12818.
27. Kraulis, P. J. (1991) MolScript: A program to produce both detailed and schematic plots of protein structures, *J. Appl. Crystallogr. 24*, 946−950.
28. Merritt, E. A., and Bacon, D. J. (1997) Raster3D photorealistic molecular graphics, *Methods Enzymol. 277*, 505−524.

BI048342V